molecules

MDPI

Article

Bichromatic Photoassociation Spectroscopy for the Determination of Rotational Constants of Cs_2 0_u^+ Long-Range State below the $6S_{1/2} + 6P_{1/2}$ Asymptote

Jizhou Wu [1,2], Jie Ma [1,2,3,*], Yuqing Li [1,2], Wenliang Liu [1,2], Peng Li [3] and Vladimir B. Sovkov [1,4,*]

1 State Key Laboratory of Quantum Optics and Quantum Optics Devices, Institute of Laser Spectroscopy, Shanxi University, 92 Wucheng Road, Taiyuan 030006, China; wujz@sxu.edu.cn (J.W.); lyqing2006@sxu.edu.cn (Y.L.); liuwl@sxu.edu.cn (W.L.)
2 Collaborative Innovation Center of Extreme Optics, Shanxi University, 92 Wucheng Road, Taiyuan 030006, China
3 College of Physics and Electronic Engineering, Shanxi University, 92 Wucheng Road, Taiyuan 030006, China; lip@sxu.edu.cn
4 Department of Photonics, St. Petersburg State University, 7/9 Universitetskaya Nab., 199034 St. Petersburg, Russia
* Correspondence: mj@sxu.edu.cn (J.M.); v.sovkov@spbu.ru (V.B.S.); Tel.: +86-351-7018-215 (J.M.)

Academic Editors: Christian G. Parigger and Robert Splinter
Received: 11 August 2020; Accepted: 28 August 2020; Published: 31 August 2020

Abstract: This article demonstrates new observation of the high-resolution ro-vibrational bichromatic photoassociation spectra (BPAS) of Cs_2 in the 0_u^+ long-range state below the asymptotes $6S_{1/2} + 6P_{1/2}$. By combining with a modulation spectroscopic technique, precise references of the frequency differences have been engineered through the BPAS, with which the rotational constants of low-lying vibrational levels of the Cs_2 0_u^+ long-range state have been accurately determined by fitting the frequency differences to the non-rigid-rotor model. The rotational constants for the newly observed seven ro-vibrational levels are summarized and disagreement for the level $\tilde{v} = 498$ is clarified. The rotational constants of different vibrational levels demonstrate strong perturbations of the related energy structures. A simple analysis is performed and shows good agreement with experimental results.

Keywords: ultracold molecule; diatomic molecules; molecular spectra; bichromatic photoassociation spectroscopy; long-range state; non-rigid-rotor model; rotational constants

1. Introduction

During trecent decades, quantum science and technologies have reached tremendous achievements benefiting from the ultracold atoms and molecules with a temperature extremely lower than 1 mK [1,2], under which the inter-particle collisions are fully quantum-mechanical and highly sensitive to long-range interactions. The straightforward preparation of an ultracold molecular sample is a challenging task, much harder than the production of ultracold atomic ensembles. The rich and complicated ro-vibrational energy level structure of molecules leads to a limited number of produced molecules and suppressed low phase-space densities obtained by direct cooling or laser cooling techniques, in which the temperature of molecules has not typically reached below ~μK [3]. Ideal (high-phase-space-density, low-temperature below 1 mK) gases of ultracold molecules can be produced from ultracold alkali atomic gases with indirect approaches such as photoassociation (PA) [4] or the magnetoassociation over a Feshbach resonance [5] followed by a Stimulated Raman Adiabatic Passage (STIRAP) [6] to deeply bound ground states [7]. Various robust and exquisite control

techniques have enabled the ultracold molecules as promising candidates in extensive applications, such as precision measurement [8], cold-reaction chemistry [9], high-resolution spectroscopy [10], quantum information processing [11], and quantum simulation [12].

Due to its relatively low requirements for the initial temperature and density parameters of atomic samples, the PA has been proven to be a versatile and simple method to prepare weakly bound ultracold molecules at the micro-Kelvin range, both for homonuclear and heteronuclear molecules [4,13,14], which demonstrate van der Waals potentials proportional to $1/R^3$ or $1/R^6$ (where R is the inter-nuclear distance) in their excited molecular states at large internuclear separations. Also, ultracold molecules prepared by PA are characterized by small binding energies as the molecules are mostly formed in the near dissociation region. Furthermore, high-resolution Photoassociation Spectroscopy (PAS) greatly reduces the Doppler Effect, thereupon the detection accuracy can be enhanced to several kHz [15–19]. In this sense, the PAS is often advantageous in the detection of molecular ro-vibrational energy levels and hyperfine structures over traditional thermo-luminescence spectroscopy or fluorescence spectroscopy techniques [20]. PAS has enabled one to obtain information of molecular structures [21], to determine the long-range behaviour of the potential energy curves and molecular constants [22,23], and to measure the s-wave scattering lengths [4] as well as the time variations of fundamental physical constants [24].

Many experimental and theoretical studies were made on the long-range states of ultracold Cs_2 molecules observed by the PA [25–34]. Firstly, the P. Pillet's research group realized the formation of the ultracold Cs_2 ground state molecules via the PA, obtained the PAS, and estimated the rotational constants for the vibrational levels of the 0_u^+ and 1_g states ranged from -5 cm^{-1} to -40 cm^{-1} relative to the Cs_2 $6S_{1/2} + 6P_{3/2}$ dissociation limit [25]. M. Pichler and co-workers reported the spectroscopic studies of the Cs_2 molecular excited states with the detuning of up to 56 cm^{-1} from the limits $6S_{1/2} + 6P_{3/2}$ [33] and $6S_{1/2} + 6P_{1/2}$ [34]. Recently, the spectroscopic detection detuning range has been extended to 70 cm^{-1} below the Cs_2 $6S_{1/2} + 6P_{3/2}$ [21] asymptote by our group. Specifically, efforts have been made to further extend the PAS detection range, both to the high-lying molecular vibrational levels within the extremely dense states and to the lower-lying levels that are largely red detuned against the $6S_{1/2} + 6P_{3/2}$ [15,18] $6S_{1/2} + 6P_{1/2}$ [35] asymptotes. However, the rotational constants of the Cs_2 0_u^+ levels below the dissociation limit $6S_{1/2} + 6P_{1/2}$, stemming from an $A^1\Sigma_u^+ \sim b^3\Pi_u$ complex in the Hund's case (a) notation, so far have not been comprehensively investigated.

In this paper, we demonstrate accurate measurements of the rotational constants of the vibrational energy levels of the ultracold Cs_2 molecules with high sensitivity. In our scheme, we have combined a new laser scan calibration scheme with modulation spectroscopy for the trap-loss fluorescence detection, thus leads to an appreciably improved signal-to-noise ratio. The scheme relies on calibrating frequency offsets within each laser scan. Partial output of the PA laser has passed through an acousto-optic modulator (AOM) to provide a calibration beam offset by 220 MHz. By mechanically switching from the main beam to the calibration beam during a laser frequency scan, a selected spectral feature can be scanned twice, namely bichromatic photoassociation spectroscopy (BPAS), with a known separation of 220 MHz that is used to calibrate the rest of the spectrum. The BPAS for specific vibrational levels in the Cs_2 0_u^+ long-range state near the dissociation limit $6S_{1/2} + 6P_{1/2}$ are newly detected, with which the rotational constants are obtained with a high accuracy. The method proposed in this paper has benefitted a correction of the previously measured rotational constants for a specific ro-vibrational level. The simple analysis demonstrates the strong perturbation effect of the 0_u^+ state. Our results provide a framework for future works exploring the precise potential energy curves of the long-range states.

2. Experimental Details

The experimental scheme for the measurement of the BPAS of ultracold Cs_2 molecules is similar to the one reported in Ref. [18], as demonstrated schematically in Figure 1. The ultracold cesium atoms were prepared by the magneto-optical-trap (MOT) technology in a vacuum chamber with a background pressure of 3×10^{-7} Pa. The trapping light and the re-pumping light were provided by

two semiconductor lasers, whose frequencies were stabilized with the standard saturated-absorption technology. The trapping laser power of totally ~39 mW was equally divided into three pairs of beams, which were transmitted through the optical fiber into the center of the cell with mutually opposite circular polarizations. A pair of anti-Helmholtz coils generated a quadrupole magnetic field along the axis of the coils with a gradient of ~16 Gauss/cm to trap the cooled ultracold cesium atoms. The repumping laser beam with a power of ~5 mW directly illuminated the MOT after the collimation of the fiber. The temperature of the ultracold cesium atomic cloud was ~200 μK, measured by the time-of-flight method. The number of atoms was ~5.1×10^7 with a characteristic diameter of the cloud of ~800 μm. The cesium MOT was monitored in real time by a Charge Coupled Device (CCD) camera (MintronMTV-1881EX).

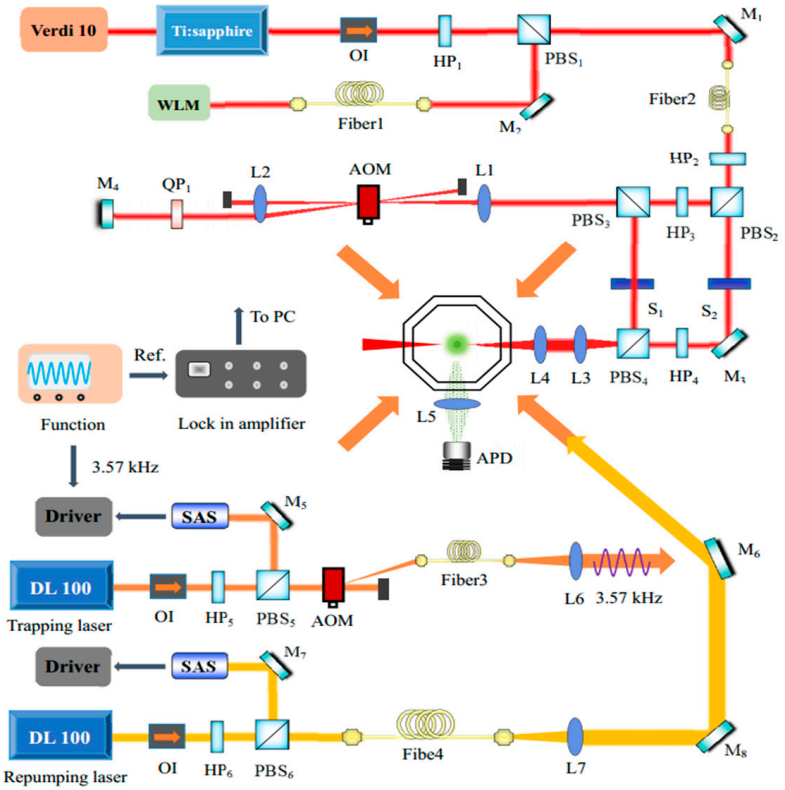

Figure 1. Experiment setup: OI: optical isolator; H: halfwave plate; PBS: polarization beam splitter; AOM: acousto-optic modulator; L: lens; M: high reflective mirror; S: shutter; Q: quarter-wave plate; APD: avalanche photodiode; SAS: saturation absorption spectroscopy; PC: computer.

A continuous tunable Ti:sapphire laser (MBR110, linewidth ~0.1 MHz, power ~1.2 W), which was pumped by a diode-pumped solid-state laser (Verdi 10, ~10 W) with an output at 532 nm, served as the PA laser. In the experiment, a commercial wavelength meter (High Finesse-Angstrom WS/7R, absolute accuracy ~60 MHz) was used to monitor and measure the absolute PA laser frequency. The cesium atomic hyperfine resonance transition, $6S_{1/2}$ (F = 3) → $6P_{1/2}$ (F′ = 4), corresponding to the wavenumber of ν_D = 11178.151 cm^{-1}, was referred to the calibration of the wavelength meter. The PA acts on two colliding ultracold atoms resonantly absorbing a photon with frequency ν to form a weakly bound excited state molecule, which spontaneously decays (lifetime ~15 ns) into the ground state or de-excites to two free atoms escaping from the MOT. Both decaying channels lead to the instantaneous loss of the ultracold atoms from the MOT. The PAS directly illustrates the number of the produced excited molecules by recording the variation of the fluorescence of the MOT, i.e., the trap loss, as a function of ν. The trap loss detection method is typically advantageous over the ionization method by providing both the frequency positions of the PA resonances and the transitional strengths, which is important for studying the PA process and optimizing the energy schemes in the STIRAP experiments but not always

available by the ionization method. The fluorescence was collected by a convex lens and detected by a silicon avalanche photodiode (APD S3884) with two pieces of 850 nm band-pass filters.

The traditional direct fluorescence spectroscopic technology usually suffered from a poor signal-to-noise ratio and low detection sensitivity due to the presence of various stray light and noise in the MOT. A lock-in method, based on modulating the fluorescence of the cesium atoms, was used to improve the detection sensitivity of the trap loss spectroscopy in our experiment. The trapping laser frequency was modulated by an auxiliary signal with a frequency of 3.57 kHz, which was also used to stabilize the laser's frequency. The modulated fluorescence was collected through an APD, demodulated by a lock-in amplifier (SR830), and recorded by a computer.

On the other hand, the BPAS technology constructs the accurate frequency reference standards and measures the frequency intervals of neighboring rotational levels with the improved precision benefitting from the modulation technique. In this way, the rotational constants of the ultracold Cs_2 molecules were obtained. The output of the PA laser was divided into two beams by passing through a half-wave plate (HP2) and a polarization prism beam splitter (PBS2). The frequency of one beam (Beam II) was reduced (shifted downwards) from the one of the main beam (Beam I) by $\Delta\nu_0 = 220$ MHz via an AOM-based double-pass configuration (the carrier frequency of the AOM was set as 110 MHz).

3. Results and Discussion

In the experiment, the typical bichromatic PA spectrum was recorded by alternately alternately shining the Beam I and Beam II from the PA laser on the MOT. The ro-vibrational PA spectrum for the rotational quantum number from $J = 0$ to 6 was firstly obtained by the trap loss that was induced by the Beam I. As the whole loss spectrum for $J = 6$ was acquired, Beam I was switched off. Then Beam II simultaneously switched on, which interacted with the MOT and, in turn, induced an atomic loss. In other words, the $J = 6$ level was first scanned by Beam I and then by Beam II. The losses induced by Beam II was denoted as J′ in order to not cause confusion. Beams I and II were set with the same intensity and well overlapped in space before interacting with the cesium MOT. Two shutters were used to independently control the two beams. The switching of the two beams was controlled by the shutters in a much shorter time (<3 ms) than the loading time (~8 s). Therefore, it did not cause significant changes in the fluorescence, except the spike in Figure 2 inset. It should be noted that the BPAS scheme strictly relies on the high linearity of the scanning rate of the PA laser, which was monitored in real time using the wavelength meter (WS/7R).

Figure 2 demonstrates the BPAS of the vibrational levels $\tilde{v} = 558, 550, 542, 530, 522, 510$, which are red detuned from the Cs_2 $6S_{1/2} + 6P_{1/2}$ dissociation limit. The $\tilde{v}$ designation is for an ordinal number of a level starting from $\tilde{v} = 0$ at the bottom of the $A^1\Sigma_u^+ \sim b^3\Pi_u$ mixing [28–30]. It is worth noting that the notation is the same as that of Ref. [31], while other reports [31,32,34] usually using the notation of $[v_D] - v$, where $[v_D] = 710$, is the virtual vibrational quantum number at the dissociation limit of the near-dissociation theory. An estimate of v_D differs in different analyses [31–33] and depends on its interpretation (which levels are counted). Further on, we used our latest result in Ref. [31]: $[v_D] = 710$ with all the coupled states of the symmetry 0_u^+ below $6S_{1/2} + 6P_{1/2}$ counted. We would also like to emphasize that in the context of the present article, this value is only needed for the level identifications and does not influence any other physically significant consequences. The binding energies T_v of specific levels are listed in Table 1. $T_v = \nu - \nu_D$, where the ν is the PA laser frequency of a specific energy levels. The spectra show similar intensity undulations on account of the Franck-Condon factors (FCFs), i.e., the photoassociation transitions between the initial scattering state and the final ro-vibrational levels in the long-range 0_u^+ states. The $J = 0$–6 spectra possess high resolution. The intensity of the spectral lines corresponding to these rotational energy levels gradually increases from $J = 0$ to the maximum value at $J = 2$, then gradually decreases to $J = 6$. The rotational progressions of higher-order terms stem from the higher orbital angular momentum contributors (*p*-wave or *d*-wave) than the *s*-wave component.

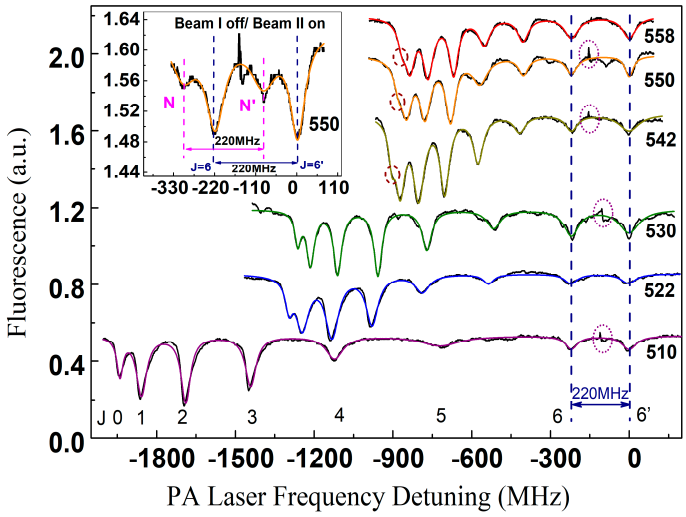

Figure 2. Six typical BPAS of the vibrational levels $\tilde{v}$ = 558, 550, 542, 530, 522, 510, of ultracold Cs_2 0_u^+ ($6S_{1/2}$ + $6P_{1/2}$) long-range state. The intensities of the PA laser beams (I and II) were 56 W/cm^2 and kept unchanged. The Ti:sapphire laser slowly scanned with stringent linearity. The colorful curves are the multipeak Lorentzian fits. The J = 0 rotational progressions for the levels with small binding energies, which are usually quite close to the J = 1 ones, are denoted as circles. The influences on the fluorescence due to the switch of the shutters are shown in the ellipses. The case for $\tilde{v}$ = 550 progression is zoomed in the inset, where the N and J = 6 indicate the spectrum produced by the Beam I scans, while N' and J' = 6 are for the Beam II scans. The N feature could stem from the strong perturbation [36] from the neighboring 0_g^- and 1_g states. Actually, in previous studies on the Cs_2 0_g^- ($6S_{1/2}$ + $6P_{1/2}$) long-range state [35], we had also observed the same phenomena. The separation between the N and N' features is $\Delta\nu_0$ = 220 MHz, as expected.

Table 1. Rotational constants B_v and centrifugal distortion constants D_v of 7 low-lying ro-vibrational levels in the 0_u^+ state below the Cs_2 dissociation limit $6S_{1/2}$ + $6P_{1/2}$. The numbering of the levels [v_D]-v from Ref. [34] has been corrected [32] in the current study and has been assigned as $\tilde{v}$, as listed in the table. The binding energies T_v, are related to J = 2 of each level, whose PA laser frequencies have also been provided as ν. The $\tilde{v}$ = 510 case is listed for reference, $\tilde{v}$ = 498 has been corrected compared to former studies [31].

$\tilde{v}$	[v_D]-v [32]	[v_D]-v [34]	T_v, J = 2 (cm^{-1})	B_v (δB_v) (MHz)	D_v (δD_v) (MHz)	ν, J = 2 (cm^{-1})
558	152	157	−7.612	15.92 (2.12)	0.04 (0.02)	11,170.539
550	160	165	−10.126	16.09 (2.53)	0.05 (0.04)	11,168.025
542	168	173	−13.480	16.52 (2.42)	0.04 (0.02)	11,164.671
530	180	185	−20.046	24.41 (1.98)	0.03 (0.02)	11,158.105
522	188	193	−26.120	25.29 (2.82)	0.06 (0.03)	11,152.031
510	200	205	−37.312	40.25 (2.02)	0.07 (0.05)	11,140.839
498	212	217	−51.488	53.57 (1.67)	0.05 (0.02)	11,126.663
494	216	221	−57.617	48.29 (2.34)	0.18 (0.04)	11,120.534
487	223	228	−68.854	53.34 (2.09)	0.15 (0.03)	11,109.297

The rotational level J = 6 was scanned by the Beam II, which was denoted as J' = 6, after the Beam I scanned it. The two beams were separated by a fixed frequency difference $\Delta\nu_0$ = 220 MHz, which was set via the AOM with an accuracy of ~kHz. To shield the influences of laser-induced frequency shifts [37] of individual levels that could lead to inaccuracy of the measurements, the two beams were adjusted within the same intensities. Thus, the frequency interval between J = 6 and J' = 6 was exactly $\Delta\nu_0$ = 220 MHz, i.e., the fixed frequency difference between the Beam I and Beam II, which was used as a precise reference to calibrate the frequency separations $\Delta\nu_J$ between neighboring

rotational levels in the BPAS. By fitting the data of $\Delta\nu_J$ to the rotor model [38], the rotational constants of specific vibrational levels, which are listed in Table 1, were obtained with high sensitivity. Compared to previous studies [18,34], the signal to noise ratio (SNR) of the current investigation was improved to ~60, and the improved sensitivity has led to an enhanced accuracy of the measurements.

In Figure 3, we show the case for $\tilde{v}$ = 498, i.e., [v_D]-v = 217 in Ref. [34]. It should be noted that in the previous studies [31], there was a misprint in Table 1, i.e., the ro-vibrational level $\tilde{v}$ = 499 should be 498, whose rotational constant was reported as 77.48 ± 0.42 MHz. This value looks excessively large, as Figures 4 and 5 show, compared to the value reported in Ref. [34]. We systemically tested the former experimental data as we carried out in Ref. [31] and found that the data for that level was wrongly processed with mistaken $\Delta\nu_0$ = 215 MHz instead of 220 MHz. In the current study, we have rescanned this level again and processed the data carefully and found that the corrected rotational constant for $\tilde{v}$ = 498 should be 53.57 ± 1.67 MHz. The BPAS of this level has been demonstrated in Figure 3. The influence from the gain of the accuracy of this level on the molecular potential energy curve, which is not the main theme of the current study, will be estimated by compared to the analysis in Ref. [36]. It is worth mentioning that we have extended the investigations to $\tilde{v}$ = 494 and 487, whose BPAS have also been exhibited in Figure 3. The extension of the BPAS, as well as the B_v constant estimates, of the 0_u^+ state far from the dissociation limit $6S_{1/2}$ + $6P_{1/2}$, will be performed in future studies. Signals for the rotational progressions with higher than J = 5, 6 with lower signal amplitudes are not considered in the present work.

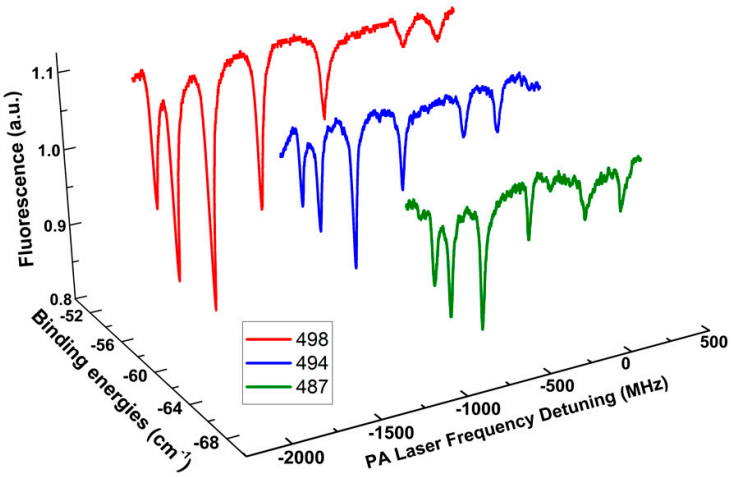

Figure 3. BPAS of the vibrational levels $\tilde{v}$ = 498, 494 and 487 of ultracold Cs_2 0_u^+ ($6S_{1/2}$ + $6P_{1/2}$) long-range state. The spectroscopy data have been extended to a red detuning of nearly ~70 cm^{-1} below the $6S_{1/2}$ + $6P_{1/2}$ dissociation limit.

The non-linear relationship between frequency intervals $\Delta\nu_J$ and J for different vibrational levels in the Cs_2 0_u^+ state below the $6S_{1/2}$ + $6P_{1/2}$ dissociation limit, which originated from the molecular long-range interaction between the two constituent atoms, is demonstrated in Figure 4. When fitting the data, we have considered the rigid-rotor model and the non-rigid-rotor model. The rigid rotor model can be considered to be the 0th order description of a molecule rotational motion, which neglects the coupling to the vibrational motion and the fact that rotating molecules do not behave as rigid-body. Thus, the rigid rotor model is often employed to describe low-J transitions of weakly bound molecular complexes. On the other hand, the non-rigidity of the molecular bonds and the vibrational-rotational interaction makes centrifugal distortion non-negligible. In particular, the ultracold Cs_2 molecule formed by the photoassociation is mainly located in the long-range state with a very large inter-nuclear distance. Therefore, the centrifugal distortion effect are important for the description of rotational transitions at increasing J quantum numbers, where the larger rotational energy causes a measurable distortion of the molecule and hence a departure of the energy levels from the rigid-rotor pattern, as the inset of Figure 4 shown. In this way, the fittings of $\Delta\nu_J$ were performed by using the molecular non-rigid-rotor

rotor model [38], the results are shown as curves of different colors in Figure 4. This model implements the following equation:

$$E_J/hc = B_v J\ (J + 1) - D_v J^2\ (J + 1)^2 \quad (1)$$

where E_J is the rotational energy, h is the Planck constant, c is the speed of light, B_v is the rotational constant, and D_v is the centrifugal distortion constant. The formula of adjacent frequency interval used for fitting is as follows:

$$\Delta\nu_J = (E_{J+1} - E_J)/hc = 2B_v(J + 1) - 4D_v\ (J + 1)^3 \quad (2)$$

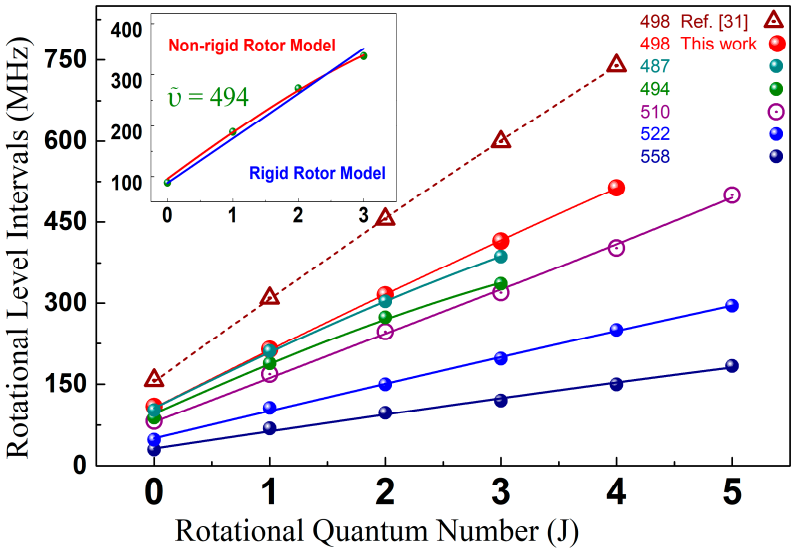

Figure 4. Relationship between J and the frequency rotational intervals Δν for specific ro-vibrational levels in the Cs_2 0_u^+ state. Experimental data, shown in colorful symbols were fitted by the nonlinear non-rigid-rotator model. The former incorrect calibrated values for $\tilde{v}$ = 498 [31], which were misprinted as $\tilde{v}$ = 499 in the reference, are also presented as triangles for comparison.

The values of B_v and D_v can thus be obtained by fitting the accurate rotation level intervals to Equation (2). As D_v is three orders smaller than B_v, it usually does not play an important role in the analysis; thereupon we only report the B_v value. These B_v and their estimated inaccuracies for specific vibrational levels are listed in Table 1. The uncertainty mainly came from the determination of the resonant peak position and the statistical error of fitting. In this analysis, the positions of the lines are taken as given by the location of their maximum. However, lines profiles are complicated, influenced by hyperfine interactions, natural linewidth, partial wave dependency, etc. [21,39]. Therefore, we did not try here to estimate the deperturbed line positions. Consequently, the rotational constants, extract from these line positions, can only be taken rough estimations of the real values and do not have any spectroscopic accuracy. The BPAS scheme and the non-rigid-rotor model enabled the accurate measurements of the molecular rotational constants.

Figure 5 illustrates the relationship between B_v values for the ro-vibrational levels of the Cs_2 0_u^+ $6S_{1/2} + 6P_{1/2}$ long-range state and the vibrational quantum numbers $\tilde{v}$. The corrected value made the high-lying vibrational levels more consistent with those for the low-lying counterpart. The current investigation reaches more accurate results than previous studies. Similar behavior of the rotational constant in the 0_u^+ state of $^{85}Rb_2$ [40] was also reported. The fluctuations of B_v values indicate a strong spin-orbit coupling between the $A^1\Sigma_u^+ \sim b^3\Pi_u$ mixing electronic states. Meanwhile, we found that the rotational constants for the Cs_2 0_g^- state below the asymptote $6S_{1/2} + 6P_{1/2}$, demonstrating a smooth variation [35], which can also be interpreted by a semi-experimental method [41], do not show the same behavior as that for the 0_u^+ state. It would be interesting to jointly analysis the different behaviors of the two long-range states through future experimental measurements and theoretical models [42] to unveil the physical mechanisms.

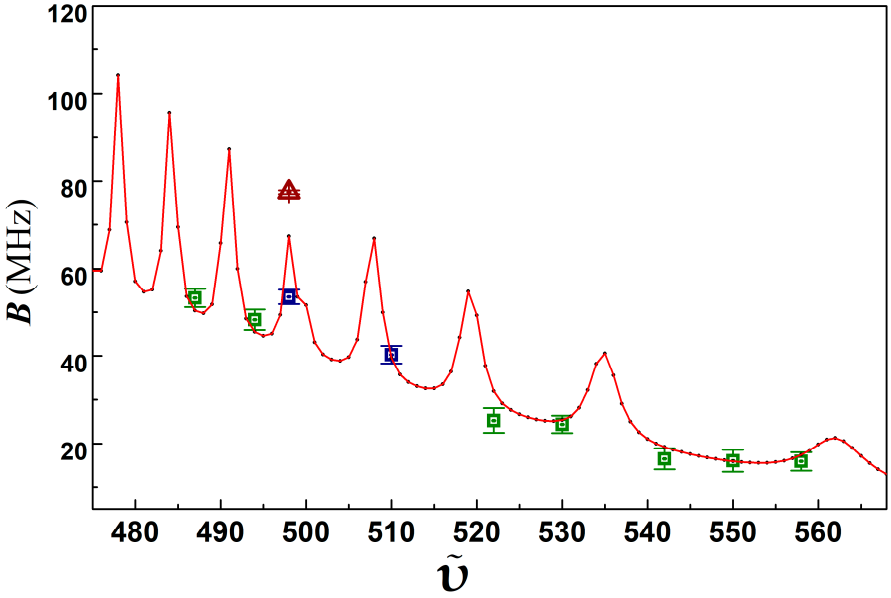

Figure 5. Rotational constants Bv of the rovibrational levels ($\tilde{v}$) in Cs_2 0_u^+ state below the dissociation limit $6S_{1/2}$ +$6P_{1/2}$. Triangle is the value reported in Ref. [31], other newly observed values are in green squares. The blue squares for $\tilde{v}$ = 498 and 510, which were observed previously, have also been measured and presented for comparison. The black dots are the theoretical rotational constants, computed in a two channel quantum mechanical simulation [31]. The solid red curve is the connection of the dots. The newly observed values are in good consistence with the theoretical curve.

4. Conclusions

In conclusion, a BPAS scheme was introduced to accurately measure the rotational constants of the ultracold Cs_2 0_u^+ long-range state below the $6S_{1/2}$ + $6P_{1/2}$ dissociation limit with high sensitivity and high resolution. A series of the BPAS spectra of Cs_2 were demonstrated. A frequency reference standard was built in combination with the modulation spectroscopic technology to acquire the frequency intervals of adjacent rotational energy levels without using a high-precision and expensive wavelength meter. The SNR as well as the sensitivity of the current research was greatly enhanced. By fitting the data to a non-rigid rotor model, which proved to be statistically significant vs. the rigid rotor one, the rotational constants of seven newly observed ro-vibrational levels were obtained. The proposed simple and robust scheme can be versatilely used to study the behaviors of other long range states of ultracold molecular species.

Author Contributions: Conceptualization, J.W. and J.M.; investigation, J.W., Y.L., and W.L.; validation, J.W., J.M., and V.B.S.; formal analysis, P.L. and V.B.S.; writing—original draft preparation, J.W.; writing—review and editing, J.W., J.M., and V.B.S.; project administration, J.W. and J.M.; funding acquisition, J.W., J.M., and V.B.S. All authors have read and agreed to the published version of the manuscript.

Funding: This research was funded by the National Key R&D program of China (Grant No. 2017YFA0304203), the National Natural Science Foundation of China (Grants Nos. 61722507, 61675121, 61705123), PCSIRT (No.IRT−17R70), 111 project (Grant No. D18001), the Program for the Outstanding Innovative Teams of Higher Learning Institutions of Shanxi (OIT), the Applied Basic Research Project of Shanxi Province (Grant No. 201801D221004, 201901D211191, 201901D211188), the Shanxi 1331 KSC and collaborative grant by the Russian Foundation for Basic Research and NSF of China (62011530047, and No. 20-53-53025 in the RFBR classification).

Conflicts of Interest: The authors declare no conflict of interest.

References

1. Kondov, S.S.; Lee, C.-H.; Leung, K.H.; Liedl, C.; Majewska, I.; Moszynski, R.; Zelevinsky, T. Molecular lattice clock with long vibrational coherence. *Nat. Phys.* **2019**, *15*, 1118–1122. [CrossRef]
2. Safronova, M.S.; Budker, D.; DeMille, D.; Jackson Kimball, D.F.; Derevianko, A.; Clark, C.W. Search for new physics with atoms and molecules. *Rev. Mod. Phys.* **2018**, *90*, 025008. [CrossRef]

3. Anderegg, L.; Augenbraun, B.L.; Bao, Y.; Burchesky, S.; Cheuk, L.W.; Ketterle, W.; Doyle, J.M. Laser cooling of optically trapped molecules. *Nat. Phys.* **2018**, *14*, 890–893. [CrossRef]
4. Jones, K.M.; Tiesinga, E.; Lett, P.D.; Julienne, P.S. Ultracold photoassociation spectroscopy: Long-range molecules and atomic scattering. *Rev. Mod. Phys.* **2006**, *78*, 483–535. [CrossRef]
5. Chin, C.; Grimm, R.; Julienne, P.; Tiesinga, E. Feshbach resonances in ultracold gases. *Rev. Mod. Phys.* **2010**, *82*, 1225–1286. [CrossRef]
6. Vitanov, N.V.; Rangelov, A.A.; Shore, B.W.; Bergmann, K. Stimulated Raman adiabatic passage in physics, chemistry, and beyond. *Rev. Mod. Phys.* **2017**, *89*, 015006. [CrossRef]
7. Ni, K.K.; Ospelkaus, S.; Miranda, M.; Peer, A.; Neyenhuis, B.; Zirbel, J.J.; Kotochigova, S.; Julienne, P.S.; Jin, D.S.; Ye, J. A High Phase-Space-Density Gas of Polar Molecules. *Science* **2008**, *322*, 231–235. [CrossRef]
8. Cairncross, W.B.; Gresh, D.N.; Grau, M.; Cossel, K.C.; Roussy, T.S.; Ni, Y.; Zhou, Y.; Ye, J.; Cornell, E.A. Precision measurement of the electron's electric dipole moment using trapped molecular ions. *Phys. Rev. Lett.* **2017**, *119*, 153001. [CrossRef]
9. Yang, H.; Zhang, D.; Liu, L.; Liu, Y.; Nan, J.; Zhao, B.; Pan, J. Observation of magnetically tunable Feshbach resonances in ultracold $^{23}Na^{40}K + {}^{40}K$ collisions. *Science* **2019**, *363*, 261–264. [CrossRef]
10. Chou, C.W.; Collopy, A.L.; Kurz, C.; Lin, Y.; Harding, M.E.; Plessow, P.N.; Fortier, T.; Diddams, S.; Leibfried, D.; Leibrandt, D.R. Frequency-comb spectroscopy on pure quantum states of a single molecular ion. *Science* **2020**, *367*, 1458–1461. [CrossRef]
11. Moses, S.A.; Covey, J.P.; Miecnikowski, M.T.; Jin, D.S.; Ye, J. New frontiers for quantum gases of polar molecules. *Nat. Phys.* **2017**, *13*, 13–20. [CrossRef]
12. Bohn, J.L.; Rey, A.M.; Ye, J. Cold molecules: Progress in quantum engineering of chemistry and quantum matter. *Science* **2017**, *357*, 1002–1010. [CrossRef] [PubMed]
13. Carr, L.D.; DeMille, D.; Krems, R.V.; Ye, J. Cold and ultracold molecules: Science, technology and applications. *New J. Phys.* **2009**, *11*, 055049. [CrossRef]
14. Ulmanis, J.; Deiglmayr, J.; Repp, M.; Wester, R.; Weidemüller, M. Ultracold Molecules Formed by Photoassociation: Heteronuclear Dimers, Inelastic Collisions, and Interactions with Ultrashort Laser Pulses. *Chem. Rev.* **2012**, *112*, 4890–4927. [CrossRef] [PubMed]
15. Ma, J.; Wu, J.; Chen, G.; Fan, Q.; Feng, H.; Dai, X.; Sun, W.; Xiao, L.; Jia, S. Experimental Determination of the Rotational Constants of High-Lying Vibrational Levels of Ultracold Cs_2 in the 0_g^- Purely Long-Range State. *J. Phys. Chem. Lett.* **2013**, *4*, 3612–3617. [CrossRef]
16. Kobayashi, J.; Ogino, A.; Inouye, S. Measurement of the variation of electron-to-proton mass ratio using ultracold molecules produced from laser-cooled atoms. *Nat. Comm.* **2019**, *10*, 3771. [CrossRef] [PubMed]
17. Altaf, A.; Dutta, S.; Lorenz, J.; Pérez-Ríos, J.; Chen, Y.P.; Elliott, D.S. Formation of ultracold $^7Li^{85}Rb$ molecules in the lowest triplet electronic state by photoassociation and their detection by ionization spectroscopy. *J. Chem. Phys.* **2015**, *142*, 114310. [CrossRef]
18. Wu, J.; Liu, W.; Li, Y.; Ma, J.; Xiao, L.; Jia, S. Experimental determination of rotational constants of low-lying vibrational levels in the 0_g^- pure long-range state of ultracold Cs_2 molecule. *J. Quant. Spectrosc. Radiate Transfer.* **2017**, *191*, 13–18. [CrossRef]
19. Dutta, S.; Pérez-Ríos, J.; Elliott, D.S.; Chen, Y.P. Two-photon photoassociation spectroscopy of an ultracold heteronuclear molecule. *Phys. Rev. A* **2017**, *95*, 013405. [CrossRef]
20. Docenko, O.; Tamanis, M.; Ferber, R.; Pazyuk, E.A.; Zaitsevskii, A.; Stolyarov, A.V.; Pashov, A.; Knöckel, H.; Tiemann, E. Deperturbation treatment of the $A^1\Sigma^+$–$b^3\Pi$ complex of NaRb and prospects for ultracold molecule formation in $X^1\Sigma^+$ ($v = 0$; $J = 0$). *Phys. Rev. A* **2007**, *75*, 042503. [CrossRef]
21. Onishchenko, S.S.; Sovkov, V.B.; Xie, F.; Li, D.; Lukashov, S.S.; Baturo, V.V.; Wu, J.; Ma, J.; Li, L. Analysis of the hyperfine structure of the Cs_2 $3^3\Sigma_g^+$ state. *J. Quant. Spectr. Radiat. Transf.* **2020**, *250*, 107037. [CrossRef]
22. Ma, J.; Wang, L.; Zhao, Y.; Xiao, L.; Jia, S. High sensitive photoassociation spectroscopy of the Cs molecular 0_u^+ and 1g long-range states below the $6S_{1/2}$+ $6P_{3/2}$ limit. *J. Mol. Spectr.* **2009**, *255*, 106–110. [CrossRef]
23. Sovkov, V.B.; Xie, F.; Lyyra, A.M.; Ahmed, E.H.; Ma, J.; Jia, S. Erratum: Re-examination of the Cs_2 ground singlet $X^1\Sigma_g{}^+$ and triplet $a^3\Sigma_u{}^+$ states. *J. Chem. Phys.* **2018**, *149*, 239901-1. [CrossRef] [PubMed]
24. Sainis, S.; Sage, J.; Kotochigova, E.T.S.; Bergeman, T.; DeMille, D. Detailed spectroscopy of the Cs_2 $a^3\sum_u^+$ state and implications for measurements sensitive to variation of the electron-proton mass ratio. *Phys. Rev. A* **2012**, *86*, 022513. [CrossRef]

25. Fioretti, A.; Comparat, D.; Crubellier, A.; Dulieu, O.; Masnou-Seeuws, F.; Pillet, P. Formation of cold Cs_2 molecules through photo-association. *Phys. Rev. Lett.* **1998**, *80*, 4402–4405. [CrossRef]
26. Bouloufa, N.; Crubellier, A.; Dulieu, O. Reexamination of the 0_g^- pure long-range state of Cs_2: Prediction of missing levels in the photoassociation spectrum. *Phys. Rev. A* **2007**, *75*, 052501. [CrossRef]
27. Jelassi, H.; Pruvost, L. Resonances in the rotational constants of 0_g^- ($6s_{1/2}$ + $6p_{1/2}$) Cs_2 levels analysed by an improved-B_v-formula associated to a 2-channel model. *Europhys. Lett.* **2016**, *115*, 43002. [CrossRef]
28. Pichler, M.; Stwalley, W.C.; Dulieu, O. Perturbation effects in photoassociation spectra of ultracold Cs_2. *J. Phys. B At. Mol. Opt. Phys.* **2006**, *39*, S981–S992. [CrossRef]
29. Dion, C.M.; Drag, C.; Dulieu, O.; Laburthe Tolra, B.; Masnou-Seeuws, F.; Pillet, P. Resonant Coupling in the Formation of Ultracold Ground State Molecules via Photoassociation. *Phys. Rev. Lett.* **2001**, *86*, 2253–2256. [CrossRef]
30. Kokoouline, V.; Dulieu, O.; Masnou-Seeuws, F. Theoretical treatment of channel mixing in excited Rb_2 and Cs_2 ultracold molecules: Perturbations in 0_u^+ photoassociation and fluorescence spectra. *Phys. Rev. A* **2000**, *62*, 022504. [CrossRef]
31. Liu, W.; Xu, R.; Wu, J.; Yang, J.; Lukashov, S.S.; Sovkov, V.B.; Dai, X.; Ma, J.; Xiao, L.; Jia, S. Observation and deperturbation of near-dissociation ro-vibrational structure of the Cs_2 state ($A^1\Sigma_u^+ \sim b^3\Pi_{0+u}$) at the asymptote $6S_{1/2}$ + $6P_{1/2}$. *J. Chem. Phys.* **2015**, *143*, 124307. [CrossRef]
32. Ma, J.; Liu, W.; Yang, J.; Wu, J.; Sun, W.; Ivanov, V.; Skublov, A.S.; Sovkov, V.; Dai, X.; Jia, S. New observation and combined analysis of the Cs_2 0_g^-, 0_u^+ and 1_g states at the asymptotes $6S_{1/2}$ + $6P_{1/2}$ and $6S_{1/2}$ + $6P_{3/2}$. *J. Chem. Phys.* **2014**, *141*, 244310. [CrossRef] [PubMed]
33. Pichler, M.; Chen, H.M.; Stwalley, W.C. Photoassociation Spectroscopy of Ultracold Cs Below the $6P_{3/2}$ Limit. *J. Chem. Phys.* **2004**, *121*, 6779–6784. [CrossRef] [PubMed]
34. Pichler, M.; Chen, H.M.; Stwalley, W.C. Photoassociation Spectroscopy of Ultracold Cs Below the $6P_{1/2}$ Limit. *J. Chem. Phys.* **2004**, *121*, 1796–1801. [CrossRef]
35. Ma, J.; Li, Y.; Liu, W.; Chen, P.; Feng, G.; Hu, C.; Wu, J.; Xiao, L.; Jia, S. Accurate determination of the rotational constants of ultracold molecules using double photoassociation spectroscopy. *Opt. Express* **2014**, *22*, 3754–3760. [CrossRef]
36. Bai, J.; Ahmed, E.H.; Beser, B.; Guan, Y.; Kotochigova, S.; Lyyra, A.M.; Ashman, S.; Wolfe, C.M.; Huennekens, J.; Xie, F.; et al. Global analysis of data on the spin-orbit-coupled $A^1\Sigma_u^+$ and $b^3\Pi_u$ states of Cs_2. *Phys. Rev. A* **2011**, *83*, 032514. [CrossRef]
37. Wu, J.; Ji, Z.; Zhang, Y.; Wang, L.; Zhao, Y.; Ma, J.; Xiao, L.; Jia, S. High sensitive determination of laser-induced frequency shifts of ultracold cesium molecules. *Opt. Lett.* **2011**, *36*, 2038–2040. [CrossRef] [PubMed]
38. Bransden, B.H.; Joachain, C.J. *Physics of Atoms and Molecules*; Longman Group Press: Essex, UK, 1983; pp. 90–102.
39. Comparat, D.; Vanhaecke, N.; Lisdat, C.; Pillet, P. Formation and Trapping of Cold Molecules. In *Interactions in Ultracold Gases: From Atoms to Molecules*; Weidemüller, M., Zimmermann, C., Eds.; Wiley-VCH Verlag GmbH & Co. KGaA: Weinheim, Germany, 2003; Chapter 11; pp. 320–336.
40. Bergeman, T.; Qi, J.; Wang, D.; Huang, Y.; Pechkis, H.K.; Eyler, E.E.; Gould, P.L.; Stwalley, W.C.; Cline, R.A.; Miller, J.D.; et al. Photoassociation of ^{85}Rb atoms into 0_u^+ states near the 5S + 5P atomic limits. *J. Phys. B* **2006**, *39*, S813–S823. [CrossRef]
41. Mendolicchio, M.; Penocchio, E.; Licari, D.; Tasinato, N.; Barone, V. Development and Implementation of Advanced Fitting Methods for the Calculation of Accurate Molecular Structures. *J. Chem. Theory Comput.* **2017**, *13*, 3060–3075. [CrossRef]
42. Tiesinga, E.; Jones, K.M.; Lett, P.D.; Volz, U.; Williams, C.J.; Julienne, P.S. Measurement and modeling of hyperfine- and rotation-induced state mixing in large weakly bound sodium dimmers. *Phys. Rev. A* **2005**, *71*, 052703. [CrossRef]

Sample Availability: Samples of the compounds are not available from the authors.